PIER C

(Received 6 April 2026, Accepted 12 May 2026, Scheduled 1 June 2026)

Compact Printed UWB Monopole Antenna Employing Coupling and Stub Structure

Nobuyasu Takemura*

Chukyo University, Japan

ABSTRACT: This paper presents a compact printed ultra-wideband (UWB) monopole antenna employing a coupling structure and a short stub for broadband impedance matching and antenna miniaturization. The proposed antenna is fabricated on an FR-4 substrate with dimensions of $24 \times 14 \times 1.6\,\text{mm}^3$ and fully covers the FCC-defined UWB from 3.1 to 10.6 GHz, achieving a VSWR of ≤ 2. The coupling structure introduces additional capacitive loading, while the short stub provides effective inductive compensation. This enables stable, broadband operation despite significant size reduction. Experimental results demonstrate quasi-omnidirectional radiation characteristics over the entire operating band. In addition to frequency-domain evaluation, time-domain performance is investigated using two identical antennas arranged in face-to-face and side-by-side configurations. The measured correlation coefficients exceed 0.94 in both configurations, and the group delay remains nearly constant at approximately 0.3 ns across the UWB. This indicates high waveform fidelity. These results confirm that the proposed antenna is well-suited for compact UWB communication systems requiring both broadband and time-domain stability.

1. INTRODUCTION

Ultra-wideband (UWB) technology has attracted sustained interest owing to its capability to support high-data-rate short-range communications, precise localization, radar sensing, and body area network applications [1, 2]. Because UWB systems rely on impulse-based or non-sinusoidal waveforms that occupy several gigahertz of bandwidth, the antenna plays a critical role in determining system performance in both the frequency and time domains. Printed monopole antennas are widely used in UWB systems because of their simple geometry, low manufacturing cost, and inherent omnidirectional radiation characteristics.

Various planar monopole configurations, including circular, elliptical, rectangular, and polygonal structures, have been reported to achieve wideband performance [3–5]. In [3], the impedance bandwidths of planar monopole antennas with different radiator shapes were systematically compared, whereas [4] and [5] demonstrated broadband characteristics achieved by combining elliptical and circular radiating elements. In addition to radiator shaping, numerous impedance-matching techniques have been proposed, such as dual microstrip feed lines, multi-feed configurations, and slotted ground planes [6–8]. For example, microstrip feeding lines with varying widths were investigated in [6], and a planar disk monopole combined with a square planar monopole using triangular feed lines was presented in [8]. In addition to geometrical optimization, several impedance-matching strategies have been introduced for UWB monopole antennas, including partial truncation of the radiator, dual-feed structures, trident-shaped feed lines, and microstrip lines with varying widths [9–12]. Recently, research efforts have increasingly focused on antenna miniaturization while preserving the wideband characteristics. Representative approaches include sector-shaped and trapezoidal unbalanced dipole antennas, corrugated planar UWB antennas, ring-slot and tapered-slot structures, and wide-slot configurations [13–17]. Other reported designs include U-shaped antennas fabricated on low-cost LCP substrates, asymmetric circular-slotted semi-circular radiators, and modified hexagonal antennas [18–20]. Furthermore, several compact UWB monopole antennas incorporating advanced design concepts have been reported, such as notched-band printed monopoles [21], circularly polarized UWB monopoles based on characteristic mode analysis [22], defected ground structure (DGS)-based wideband monopoles [23], and characteristic-mode-based design approaches that enhance the radiation and polarization stability over wide frequency ranges [24]. Circular and circular-like printed monopole antennas have been widely investigated for UWB applications due to their simple structure, broad impedance bandwidth, and quasi-omnidirectional radiation characteristics. Various approaches have been reported, including slot-loaded circular monopoles, modified ground-plane structures, and material-based radiators, such as graphene-film-based circular monopole antennas [25–27]. These studies demonstrate that circular monopole antennas are a mature and effective platform for UWB antenna design. These studies demonstrate various strategies to improve UWB antenna performance, including multiband rejection, modal optimization, ground-plane modification, and circular polarization

* Corresponding author: Nobuyasu Takemura (takemura@sist.chukyo-u.ac.jp).

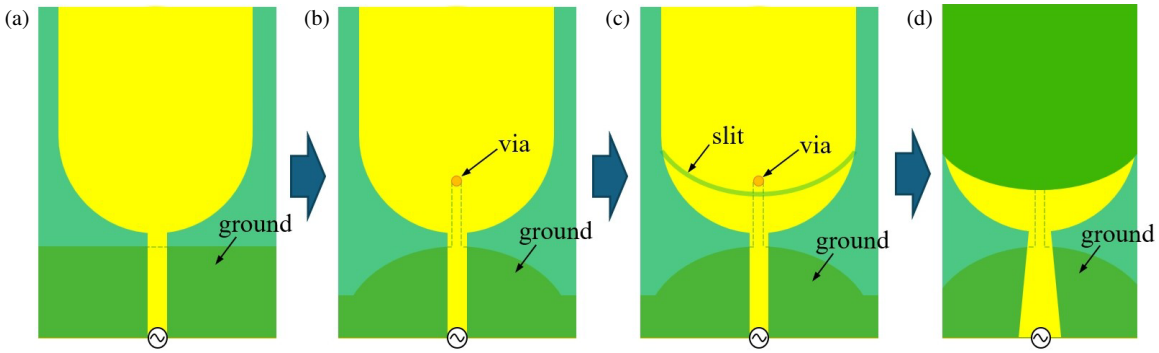

FIGURE 1. Process of UWB monopole antenna shape change: (a) UWB monopole antenna; (b) UWB monopole antenna with a short stub [28]; (c) slit added for coupling; and (d) front side conductor formed into the back side.

synthesis, while maintaining impedance matching across the FCC-defined UWB of 3.1–10.6 GHz.

In our previous studies, printed bell-shaped and half-shaped monopole antennas with short stubs were proposed to improve impedance matching in the lower UWB and to reduce the antenna footprint [28, 29]. In those designs, the bandwidth enhancement was primarily achieved by adding a short stub to the monopole radiator. However, the radiator and matching structure were still implemented primarily on both sides of the substrate, requiring a via hole, so further miniaturization remained an issue. In contrast, this study presents a coupling-and-stub configuration in which the front-side crescent-shaped radiator is electromagnetically coupled to a back-side conductor. The coupling section provides capacitive loading, and the short stub connected to the backside conductor provides reactive compensation. It should also be noted that our preliminary conference paper [30] reported only the basic design concept and initial experimental results. This journal paper significantly extends that work by providing a systematic parametric study, an equivalent circuit-based interpretation, a detailed current-distribution analysis, a radiation-pattern evaluation, a measured validation, a time-domain waveform analysis, a group-delay evaluation, and an expanded comparison with competitive UWB monopole antennas. The main contributions of this study are summarized as follows:

1) A compact printed UWB monopole antenna employing a coupling and short-stub structure is proposed, achieving approximately 40% footprint reduction compared with previously reported stub-loaded designs.

2) A systematic parametric investigation clarifies the roles of the coupling capacitance and stub inductance in broadband impedance matching.

3) Comprehensive validation is conducted, including a time-domain performance evaluation using the correlation coefficient and group-delay metrics.

The remainder of this paper is organized as follows. Section 2 describes the configuration of the proposed antenna and its operating mechanism through parametric analysis. Section 3 presents the simulated and experimental result validation using a fabricated prototype. Section 4 presents the time-domain performance evaluation results. Finally, Section 5 concludes the paper.

2. ANTENNA CONFIGURATION AND OPERATING MECHANISM

The proposed antenna is designed to achieve broadband operation and miniaturization through the combined use of a coupling structure and a short stub. Fig. 1 shows the process of the shape change of the UWB monopole antenna. First, a monopole antenna fed by a microstrip line is formed into a bell shape. Next, a short stub structure is added to the bell-shaped UWB monopole antenna [28]. This antenna consists of a short stub added from the lower center of the monopole to the ground conductor of a microstrip line. Then, a slit is made in the bell-shaped monopole, and a coupling structure is added to the antenna. Finally, the via hole above the slit on the surface of the substrate is removed, and a conductor is formed on the backside of the substrate.

Figure 2 shows the structure of the proposed UWB monopole antenna with the coupling and stub structures. The antenna is fed by a tapered microstrip feed line connected to a crescent-shaped radiator on the front side of the substrate. The remaining radiator section is implemented on the backside of the substrate and interacts with the front radiator through capacitive coupling. This coupling structure enables the surface-mount implementation of the antenna configuration without a via-hole. The radiator section on the backside and the ground conductor are connected using a stub. These structures improve the impedance matching of the UWB monopole antenna and enable wideband operation.

To provide insight into the impedance-matching mechanism, Fig. 3 shows a conceptual equivalent circuit model of a planar UWB monopole antenna with the addition of coupling and short-stub structures. The broadband impedance response of the monopole antenna can be interpreted as the superposition of multiple adjacent resonances. Therefore, the impedance of the monopole radiator can be represented by a multi-resonant network composed of parallel RLC circuits [31]. The impedance Z_M is expressed as follows.

$$Z_M = \sum_{k=1}^{n} \frac{j\omega C_k L_k}{R_k\left(1-\omega^2 L_k C_k\right)+j\omega L_k} \tag{1}$$

where R_k, L_k, and C_k $(k = 1, 2, ..., n)$ represent the equivalent resistance, inductance, and capacitance, respectively, as-

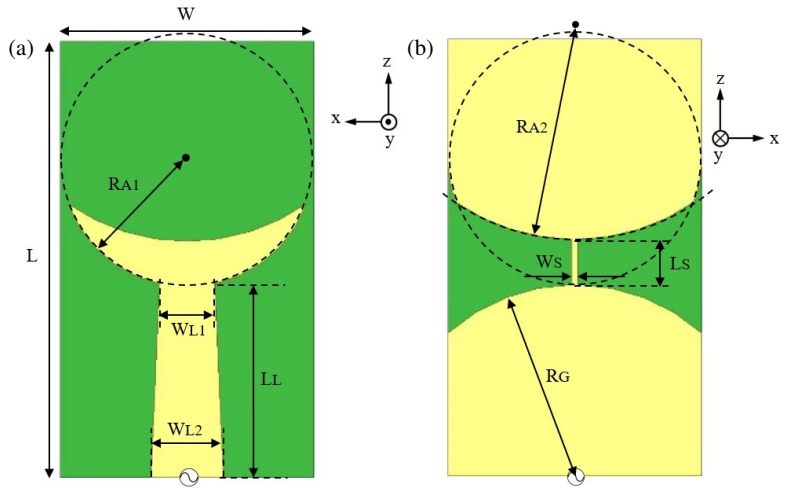

FIGURE 2. Proposed UWB monopole antenna with coupling and stub structures: (a) front view and (b) back view.

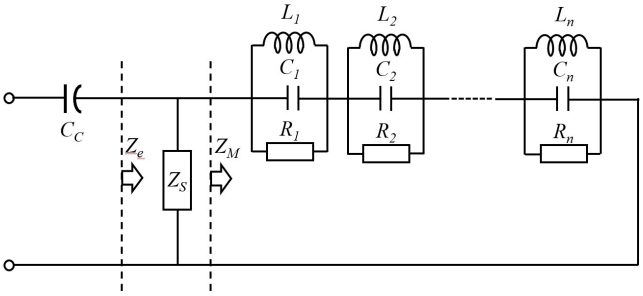

FIGURE 3. Equivalent circuit of UWB monopole antenna with coupling and stub structure.

sociated with the kth resonant mode of the monopole radiator. The proposed antenna consists of a crescent-shaped radiator on the front side and a back-side conductor that forms a capacitive coupling path. This coupling can be modeled as an equivalent capacitance (C_C). The short stub connected to the backside conductor and the ground plane provides an additional reactive current path that can be modeled as an inductive or short-stub impedance (Z_S). Therefore, the input impedance of the proposed antenna can be conceptually expressed as follows

$$Z_{in} = Z_e + j\omega C_C = \frac{Z_S Z_M}{Z_S + Z_M} + j\omega C_C \qquad (2)$$

where Z_S is the impedance of the short stub, Z_M the input impedance of the UWB monopole antenna, as shown in Equation (1), and C_C the capacitance of the coupling structure between the crescent-shaped monopole and conductor on the backside of the dielectric substrate. According to this model, the impedance of the miniaturized monopole radiator is compensated by two additional reactive mechanisms. The coupling capacitance modifies the input reactance between the front and back conductors. The short stub provides an effective low-frequency current path, compensating for the impedance degradation caused by miniaturization. Consequently, multiple resonances are brought closer together, resulting in broadband impedance matching over the UWB. The equivalent circuit in Fig. 3 is a conceptual model that illustrates the dominant resonance behavior of the antenna, not a quantitative reproduction of its full electromagnetic response. Owing to the complex, three-dimensional current distribution and multiple higher-order resonances excited in the bell-shaped monopole with a coupling and short stub, an exact circuit realization that fully matches the broadband electromagnetic (EM) characteristics would require an extensive multi-resonance network. The present circuit representation is intended to provide an understanding of how the coupling structure and short stub contribute to impedance matching.

To achieve wideband characteristics of the antenna, the antenna parameters in Fig. 2 are adjusted through a parametric study. The parameters are the stub length (L_s), stub width (W_s), cut radius of the monopole (R_{A2}), and radius of the ground plane (R_G). The default values of these parameters are $L_s = 2.5\,\text{mm}$, $W_s = 0.3\,\text{mm}$, $R_{A2} = 11.5\,\text{mm}$, and $R_G = 10.5\,\text{mm}$. The antenna is formed on an FR-4 dielectric substrate with a thickness of 1.6 mm, relative permittivity of $\varepsilon_r = 4.4$, and loss tangent of $\tan\delta = 0.02$. The size of the dielectric substrate is the length $L = 24\,\text{mm}$ and the width $W = 14\,\text{mm}$. The length and width of the tapered microstrip transmission line are $L_L = 10.5\,\text{mm}$, $W_{L1} = 3.0\,\text{mm}$, and $W_{L2} = 4.0\,\text{mm}$. The radius of the crescent-shaped monopole is $R_{A1} = 7.0\,\text{mm}$. The characteristic impedance is $50\,\Omega$.

The simulated input impedance is plotted as a function of L_s in Fig. 4, where (a) is the Smith chart, and (b) shows the corresponding reflection characteristics of the antenna. Fig. 5 compares the simulated input impedances obtained by varying the width W_s. The simulated values of the width W_s are 0.1, 0.2, 0.3, and 0.4 mm. As W_s increases, the lower frequency limit shifts to higher frequencies. Additionally, the characteristics in the mid-range tend to deteriorate. Fig. 6 compares the simulated input impedances and reflection coefficients obtained by varying cut radius R_{A2}. The simulated values of radius R_{A2} are 10.5, 11.0, 11.5, and 12.0 mm. The other parameters are the same as the default values. As R_{A2} increases, the stub length decreases, and the lower resonance frequency shifts to higher frequencies. In addition, the mid-range characteristics become worse, whereas the high-frequency characteristics tend to im-

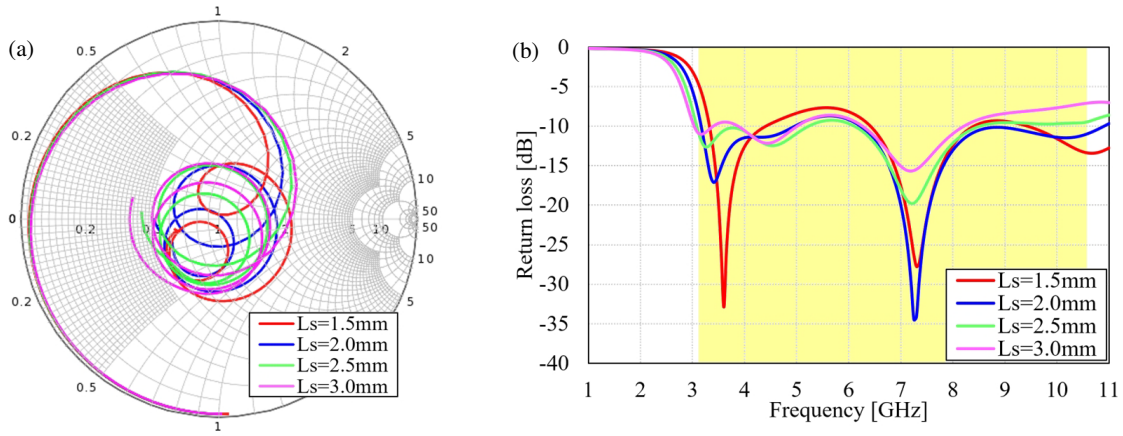

FIGURE 4. Comparison of simulated input impedance (with parameter L_s): (a) Smith chart (1–11 GHz) and (b) reflection characteristic.

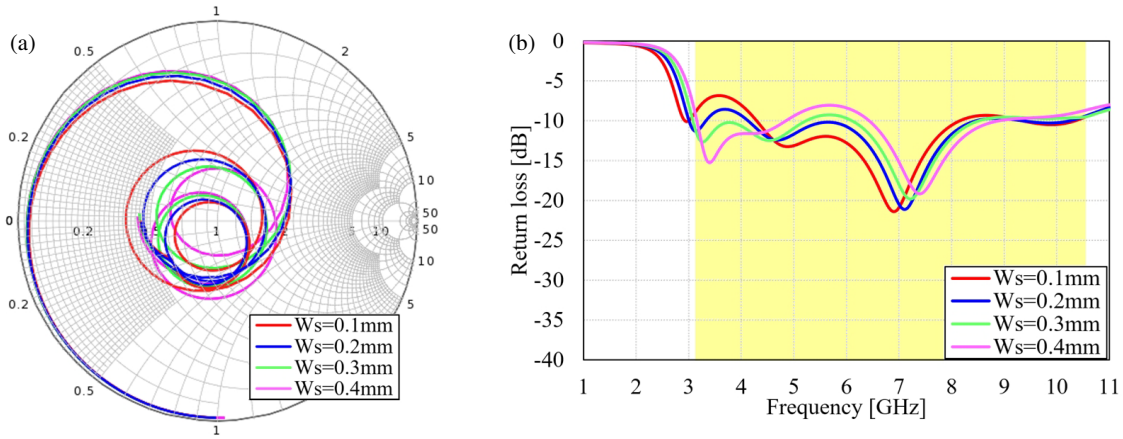

FIGURE 5. Comparison of simulated input impedance (with parameter W_s): (a) Smith chart (1–11 GHz) and (b) reflection characteristic.

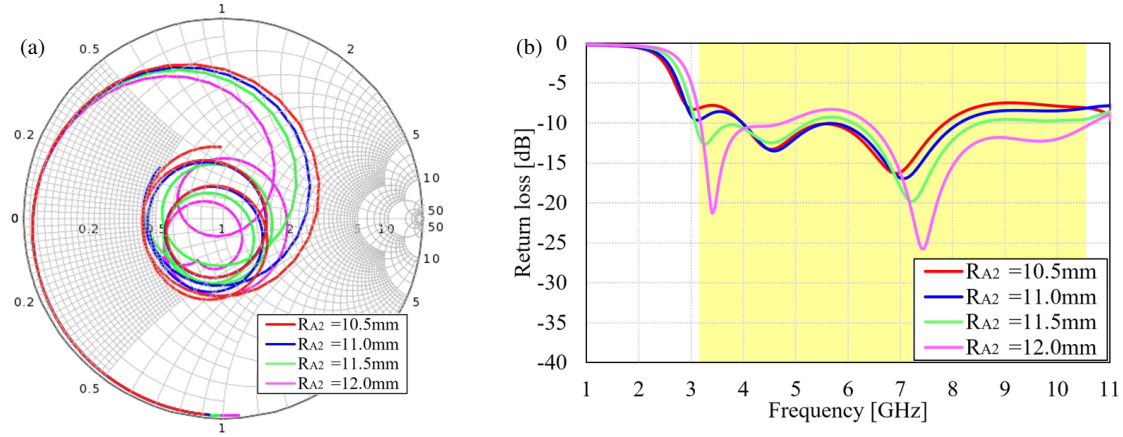

FIGURE 6. Comparison of simulated input impedance (with parameter R_{A2}): (a) Smith chart (1–11 GHz) and (b) reflection characteristic.

prove. The simulated input impedance is plotted as a function of R_G in Fig. 7.

The parametric results confirm that the coupling and stub elements are critical to broadband impedance control. The stub length L_s primarily affects the lower resonant frequency because it changes the effective current path between the radiator and the ground plane. Increasing or decreasing L_s modifies the inductive reactance of the short stub path and shifts the impedance locus on the Smith chart, especially in the lower UWB. The stub width W_s also influences the impedance-matching condition by changing the characteristic impedance and current concentration of the stub. A wider stub reduces the effective inductive behavior and tends to shift the lower operating frequency upward. Therefore, an excessive increase in

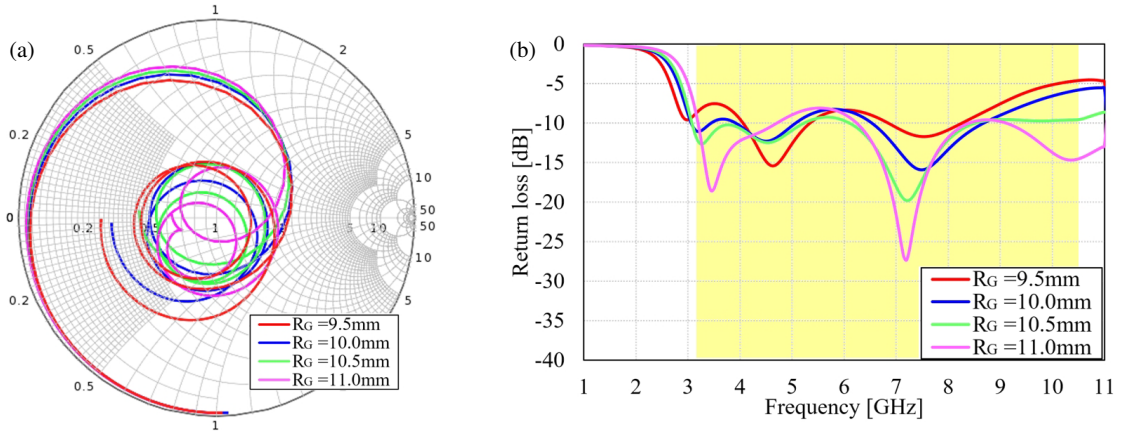

FIGURE 7. Comparison of simulated input impedance (with parameter R_G): (a) Smith chart (1–11 GHz) and (b) reflection characteristic.

W_s worsens the impedance matching in the lower and middle frequency ranges. The cut radius R_{A2} determines the shape of the crescent radiator and the coupling area between the front-side and back-side conductors. As R_{A2} changes, both the effective radiator length and the coupling capacitance change as well. This explains the observed variation in both the lower resonance and high-frequency impedance behavior. Additionally, the ground plane radius R_G affects the return current distribution, contributing to radiation pattern stability and impedance matching. These results demonstrate that the proposed antenna does not rely on a single resonance. Instead, broadband operation is achieved by controlling several adjacent resonances through the combined effects of the radiator geometry, capacitive coupling, and short-stub compensation.

3. FREQUENCY-DOMAIN PERFORMANCE

The optimal dimensions of the proposed antenna are determined based on the results of the parametric analysis presented in Section 2. The effectiveness of the proposed half-shaped, planar UWB monopole antenna is validated by a comprehensive set of evaluations combining full-wave electromagnetic simulations with experimental measurements of a fabricated prototype. The antenna is simulated using the 3D electromagnetic simulator Keysight EMPro.

3.1. Impedance Characteristics

The simulation results of the voltage standing-wave ratio (VSWR) are shown in Fig. 8. This figure shows the characteristics of the proposed antenna with the coupling and stub structures, as well as those of the conventional antenna. The conventional antenna is a printed UWB monopole antenna with a short stub structure [28]. From the simulation result of VSWR, even when the antenna is miniaturized by applying the coupling and stub structures, the VSWR characteristics are almost the same as those of the conventional antenna. The antenna characteristics satisfy VSWR ≤ 2. These results confirm the physical interpretation provided by the equivalent-circuit model, showing that the coupling and stub structures effectively compensate for the impedance degradation caused by miniaturization.

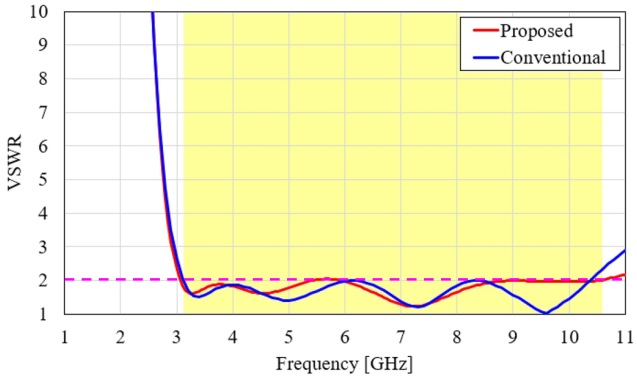

FIGURE 8. Comparison of simulated VSWR (the proposed antenna with coupling and stub structures and the conventional antenna).

3.2. Current Distribution

Figure 9 shows the simulated surface current distributions on the front and back sides of the proposed antenna at frequencies of 3.5, 4.5, 6.5, 8, 9, and 10 GHz. At lower frequencies, especially around 3.5 and 4.5 GHz, strong current concentration is observed along the short stub and the lower edge of the crescent-shaped radiator. This indicates that the short stub provides an additional current path between the radiator and the ground plane. The effective lengthening of the current path lowers the operating frequency and improves impedance matching in the lower UWB. At middle frequencies, such as 6.5 and 8 GHz, the current is distributed over the front crescent-shaped radiator and the backside conductor. This behavior indicates that the front-to-back coupling structure participates in the radiation mechanism and contributes to the formation of adjacent resonances. The capacitive coupling between the two conductors adjusts the input reactance and improves broadband matching. At higher frequencies, such as 9 and 10 GHz, the current distribution becomes more localized, exciting higher-order current modes around the edges of the radiator. While these higher-order modes slightly distort the radiation pattern, they also contribute to maintaining the impedance bandwidth at the upper end of the UWB. Thus, the results of the current distribution support the equivalent circuit interpretation that the broadband characteristic is obtained through the combined ef-

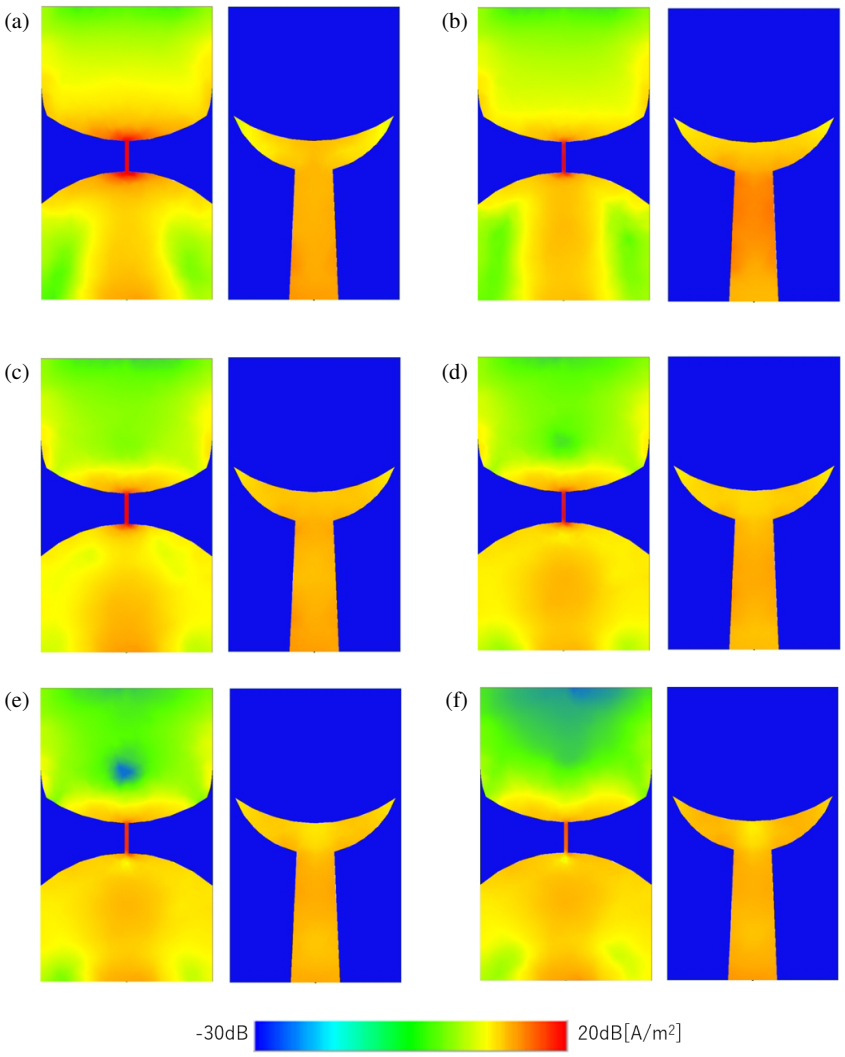

FIGURE 9. Simulation results of current distribution (front view and back view): (a) 3.5 GHz, (b) 4.5 GHz, (c) 6.5 GHz, (d) 8 GHz, (e) 9 GHz, and (f) 10 GHz.

fects of the short-stub current path and the coupling-induced capacitive loading.

3.3. Radiation Characteristics

Figure 10 shows the simulation results for the radiation pattern. Figs. 10(a) through (c) show the lower frequencies of 3.5 GHz, 4.5 GHz, and 6.5 GHz, and Figs. 10(d) through (f) show the higher frequencies of 8 GHz, 9 GHz, and 10 GHz. The radiation pattern plot is on the x-y plane. The simulation results show that almost omnidirectional radiation patterns are obtained at each frequency. Although weaker radiation is observed in the x-axis direction at higher frequencies (above 8 GHz), the overall radiation behavior remains quasi-omnidirectional. These results indicate that the antenna is capable of supporting stable communication links in environments where the device orientation varies. Although the cross-polarization levels slightly increase at higher frequencies due to higher-order modes and geometric asymmetry, the overall radiation performance remains suitable for practical UWB applications.

3.4. Measurement of Impedance Characteristics

The proposed antenna was fabricated and characterized experimentally. Fig. 11 shows photographs of the front and back views of the prototype. It is fabricated on an FR-4 dielectric substrate with a relative permittivity of $\varepsilon_r = 4.4$, and a loss tangent of $\tan\delta = 0.02$. The dimensions of the substrate are 24 mm $\times$ 14 mm $\times$ 1.6 mm. The tapered feedline parameters are $L_L = 10.5$ mm, $W_{L1} = 3.0$ mm, and $W_{L2} = 4.0$ mm. The stub dimensions are $L_s = 2.5$ mm and $W_s = 0.3$ mm. The radii of the ground plane and crescent monopole are $R_G = 10.5$ mm, $R_{A1} = 7.0$ mm, and $R_{A2} = 11.5$ mm, respectively. The antenna is designed for a characteristic impedance of 50 Ω.

Figure 12 compares the measured and simulated VSWR characteristics. The measured data agree well with the simulated results, confirming that the proposed antenna satisfies the VSWR ≤ 2 criterion across the 3.1–10.6 GHz band. These results demonstrate that the antenna provides the wideband impedance characteristics required for UWB operation.

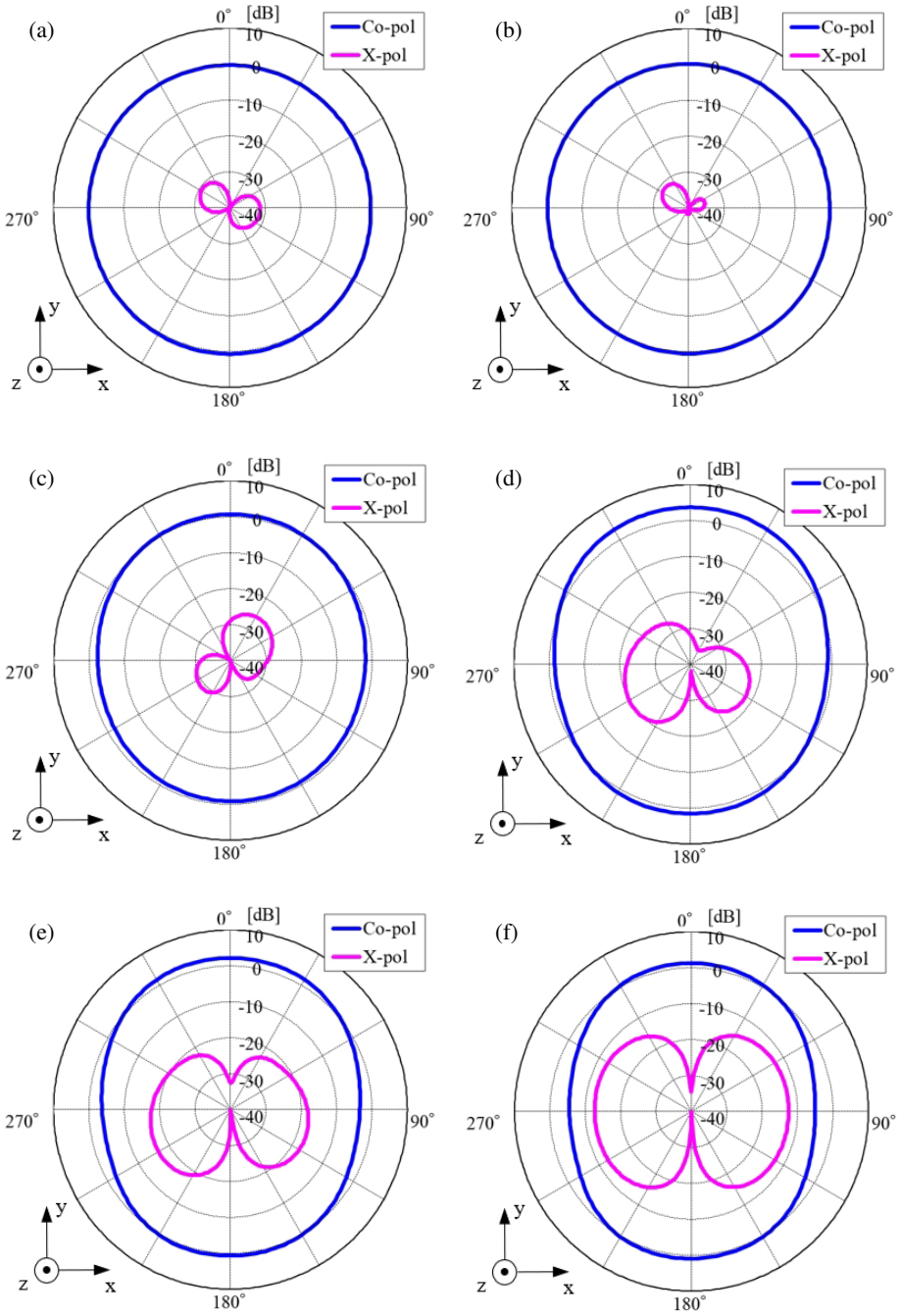

FIGURE 10. Simulated radiation patterns of the proposed antenna in the x-y plane at representative frequencies: (a) 3.5 GHz, (b) 4.5 GHz, (c) 6.5 GHz, (d) 8 GHz, (e) 9 GHz, and (f) 10 GHz.

3.5. Measurement of Radiation Characteristics

Figure 13 shows the measured radiation patterns in the x-y plane at representative frequencies of 3.5 GHz, 4.5 GHz, 6.5 GHz, 8 GHz, 9 GHz, and 10 GHz. The radiation exhibits nearly omnidirectional characteristics at all measured frequencies, which is consistent with the typical monopole behavior. These results indicate that the proposed antenna exhibits a stable radiation performance across the entire UWB frequency range. A comparison between the simulated radiation patterns in Fig. 10 and the measured radiation patterns in Fig. 13 shows that both results exhibit quasi-omnidirectional behavior over the UWB. The measured patterns reflect the general trend predicted by the simulation, especially the consistent co-polarized radiation in the x-y plane. However, at higher frequencies, the measured patterns show slightly larger ripples and cross-polarized components than the simulated results. These discrepancies are primarily due to fabrication tolerances, soldering of the SMA connector, cable effects during measurement, and the finite measurement environment. While exact agreement between the simulated and measured radiation patterns is difficult to achieve across an ultra-wide frequency range, the measured results validate the primary radiation characteristics of the proposed antenna. Therefore, the experimental results

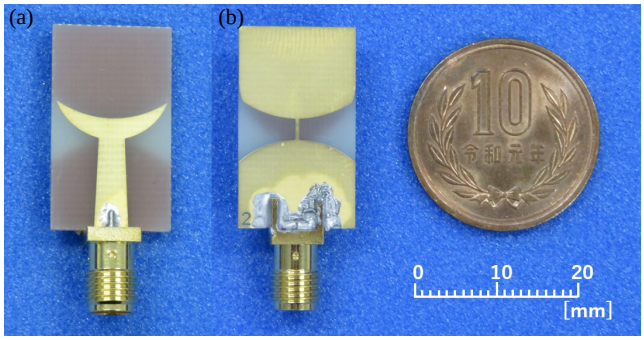

FIGURE 11. Prototype antenna: (a) front view and (b) back view.

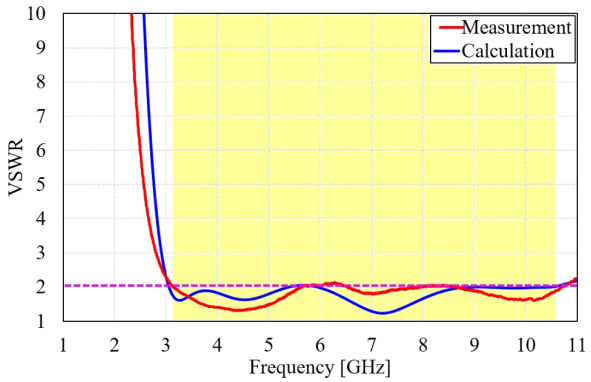

FIGURE 12. Comparison of VSWR (the measured and simulated characteristics).

support not only the impedance performance shown in Fig. 12 and the radiation stability predicted by the full-wave simulation.

These results confirm that the proposed antenna successfully achieves the two objectives of antenna miniaturization and broadband performance. Compared with a previously reported UWB monopole with a short stub, the antenna area is reduced by approximately 40%, while nearly identical bandwidth characteristics are maintained. The quasi-omnidirectional radiation patterns ensure robust system-level performance for UWB applications across the entire UWB.

4. TIME-DOMAIN PERFORMANCE

UWB systems communicate by transmitting digital signals that are converted into impulse-type or non-sinusoidal waveforms. These waveforms typically consist of sub-nanosecond pulses. When transformed into the frequency domain, these signals occupy a bandwidth of several gigahertz (GHz). To ensure reliable high-speed communication, UWB antennas must provide stable transmission and reception characteristics that are largely independent of orientation. Consequently, the time-domain fidelity of an antenna is as important as its frequency-domain impedance and radiation characteristics. In practice, an antenna with a wide impedance bandwidth in the frequency domain can still exhibit poor phase linearity or group-delay variation, which distorts the transmitted waveform. This distortion leads to inter-symbol interference and reduced data throughput. Therefore, in addition to the VSWR and radiation pattern analysis, time-domain analysis is essential to confirm that the antenna can transmit and receive UWB pulses with minimal distortion.

To study the time-domain behavior of the proposed antenna, two identical antennas were used as the transmitter (Tx) and receiver (Rx) pair. The antennas are placed 1 m apart in two different configurations: (a) face-to-face, in which the radiating surfaces are aligned along the same axis, and (b) side-by-side, in which the antennas are oriented parallel to each other but displaced laterally. These two antenna configurations are shown in Fig. 14. A distance of 1 m was selected to approximate a typical short-range indoor communication scenario while ensuring operation in the far-field region of the antenna at most frequencies within the UWB. A Gaussian pulse was used as an excitation signal. The received signals were recorded, and their temporal waveforms were compared with the transmitted signals to evaluate the signal distortion and correlation performance.

4.1. Time-Domain Analysis of Waveform

The results of the time-domain analysis are shown in Fig. 15. Fig. 15(a) corresponds to the face-to-face configuration, and Fig. 15(b) corresponds to the side-by-side configuration. A comparison of the two configurations reveals that the received amplitudes are similar for the parallel and face-to-face configurations. This indicates minimal directional bias, as the radiation patterns observed in the frequency domain simulation (Fig. 10) are symmetrical.

To quantify the waveform similarity, the correlation coefficient (ρ) between the transmitted and received signals is calculated as follows:

$$\rho = \max_{\tau} \left\{ \frac{\int S_1(t) S_2(t-\tau) dt}{\sqrt{\int S_1^2(t) dt} \sqrt{\int S_2^2(t-\tau)\, dt}} \right\} \tag{3}$$

where $S(t)$ represents the signal strength, and τ is the delay time. In the case of the face-to-face and side-by-side antenna configurations, the correlation coefficients are calculated as 0.963 and 0.947, respectively. These results confirm the high degree of similarity between the waveforms. In addition, the arrival times of the signals are nearly identical for both configurations. These results demonstrate that the proposed antenna maintains robust time-domain performance and can provide a consistent communication quality regardless of the relative orientation of the transceivers in UWB applications.

4.2. Group-Delay Characteristics

The group-delay characteristics were evaluated to investigate the phase linearity of the proposed antenna. Group delay is defined as the negative derivative of the transmission phase with respect to angular frequency. It is expressed as follows:

$$T_d = -\frac{d\theta}{d\omega} \tag{4}$$

where θ denotes the antenna phase, and ω denotes the angular frequency. For broadband communication systems, the group-delay response should exhibit minimal variation, a small phase

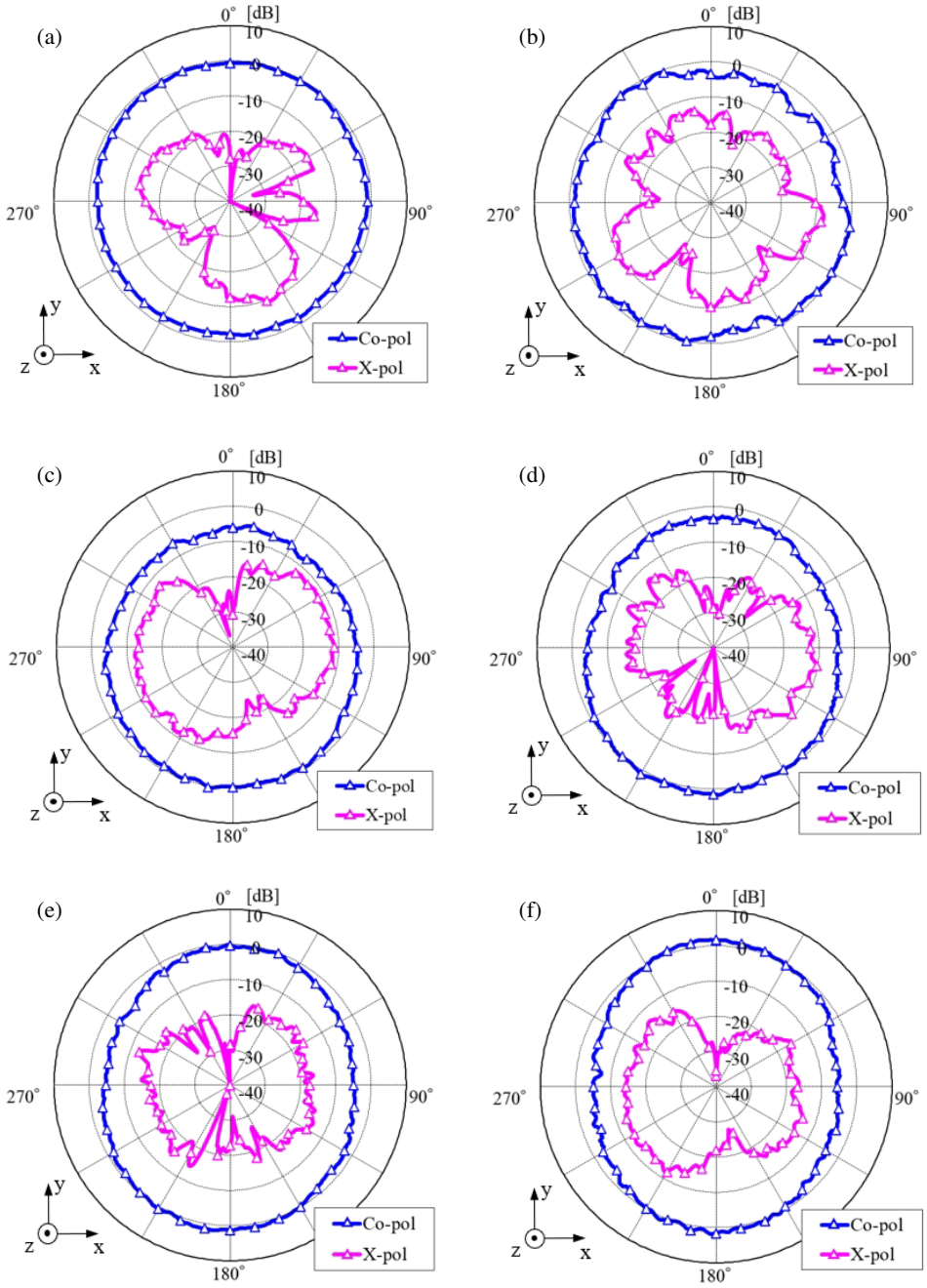

FIGURE 13. Measured radiation patterns of the fabricated antenna in the x-y plane at representative frequencies: (a) 3.5 GHz, (b) 4.5 GHz, (c) 6.5 GHz, (d) 8 GHz, (e) 9 GHz, and (f) 10 GHz.

gradient, and approximate linearity, because these features correspond to low distortion and stable signal transmission. The antenna phase is derived from the complex S-parameters as follows:

$$\theta = \tan^{-1} \frac{\mathrm{Im}(S)}{\mathrm{Re}(S)} \tag{5}$$

where $\mathrm{Re}(S)$ and $\mathrm{Im}(S)$ represent the real and imaginary components of the S-parameter, respectively. For UWB pulse transmission, a nearly constant group delay is desirable because significant variation in the group delay causes waveform distortion and inter-symbol interference. Fig. 16(a) shows the calculated phase response of S_{11}, and Fig. 16(b) shows the corresponding group-delay characteristics obtained from Equations (2) and (3). The phase response exhibits a moderately steep slope immediately following phase inversion. However, it remains predominantly linear across the operating band. Although the group delay increases slightly at frequencies corresponding to the resonant points, the overall delay remains nearly constant at approximately 0.3 ns over the entire UWB range. The calculated phase response of S_{21} and the corresponding group-delay characteristics are shown in Fig. 17. The overall delay remains nearly constant at approximately 0.6 ns over the entire UWB range. This stability confirms that the proposed antenna is well-suited for high-speed, low-distortion communication applications.

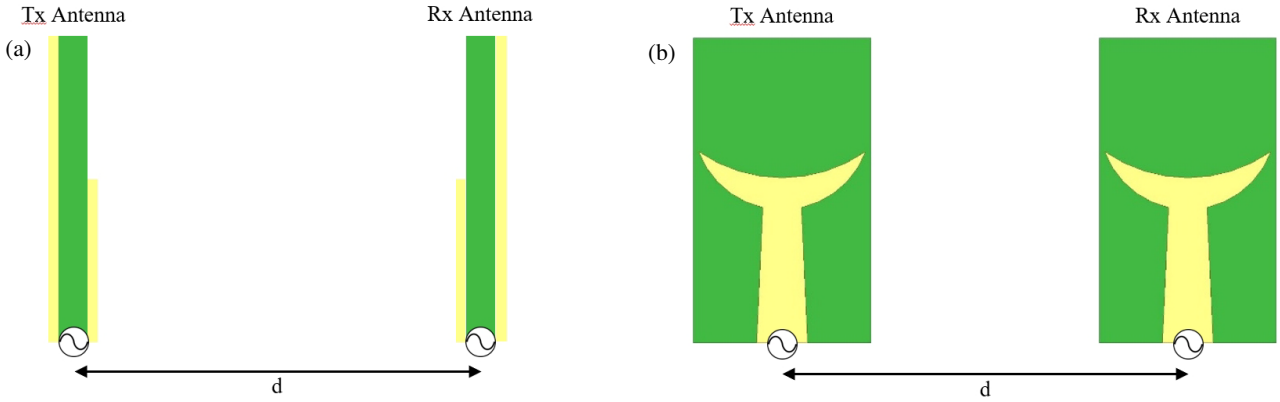

FIGURE 14. Antenna configuration: (a) face-to-face and (b) side-by-side.

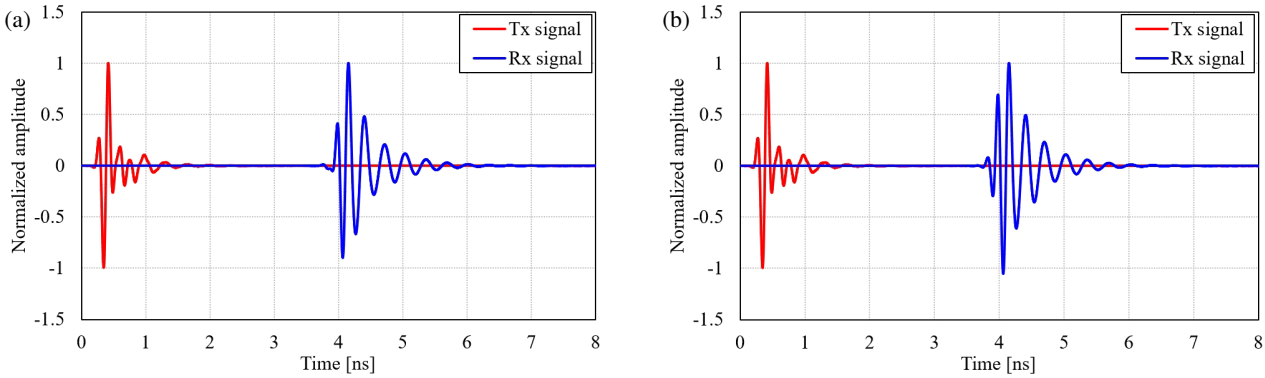

FIGURE 15. Simulated time-domain transmitted and received waveforms for two antenna arrangements: (a) face-to-face configuration and (b) side-by-side configuration.

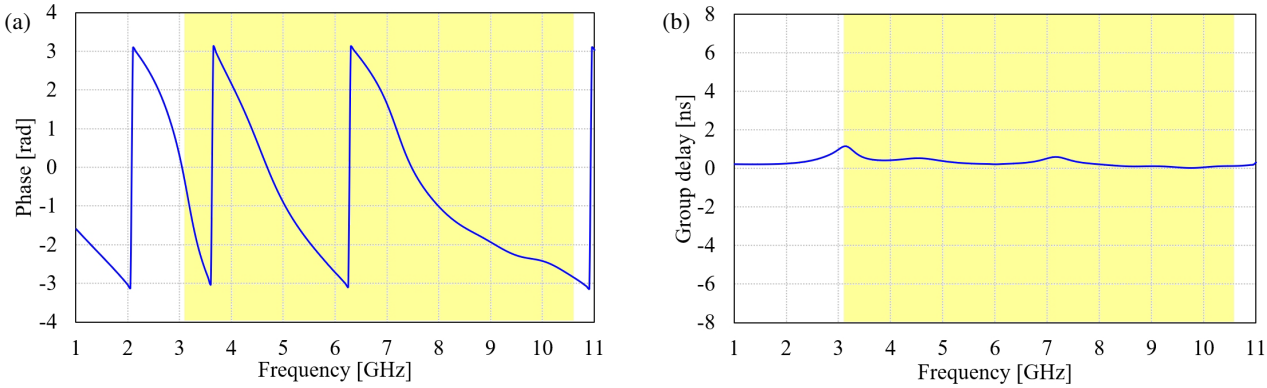

FIGURE 16. Calculated phase and group-delay characteristics of S_{11}: (a) phase and (b) group-delay.

Table 1 summarizes a comparative study of representative UWB printed-monopole antennas reported in the literature and the proposed UWB monopole antenna. To provide a fairer and more focused comparison, Table 1 compares the proposed antenna with representative compact UWB monopole antennas, with a particular emphasis on circular, circular-like, and modified planar monopole configurations. The antennas are compared based on the following key performance indicators: antenna size, substrate material, impedance bandwidth, gain or radiation efficiency, radiation pattern stability, time-domain analysis, and notable structural features used to achieve broadband characteristics. According to this comparison, many previously reported designs use conventional circular or elliptical monopoles, often combined with slots, tapered structures, or corrugated geometries to extend impedance bandwidth. Although these approaches are effective in achieving wide operating ranges, they generally require larger substrate areas and more complex fabrication processes. Several previously reported circular or modified planar monopole antennas have wider impedance bandwidths or higher gains than the proposed antenna. Therefore, the advantage of the proposed antenna is not limited to maximum bandwidth or gain. Rather, it provides

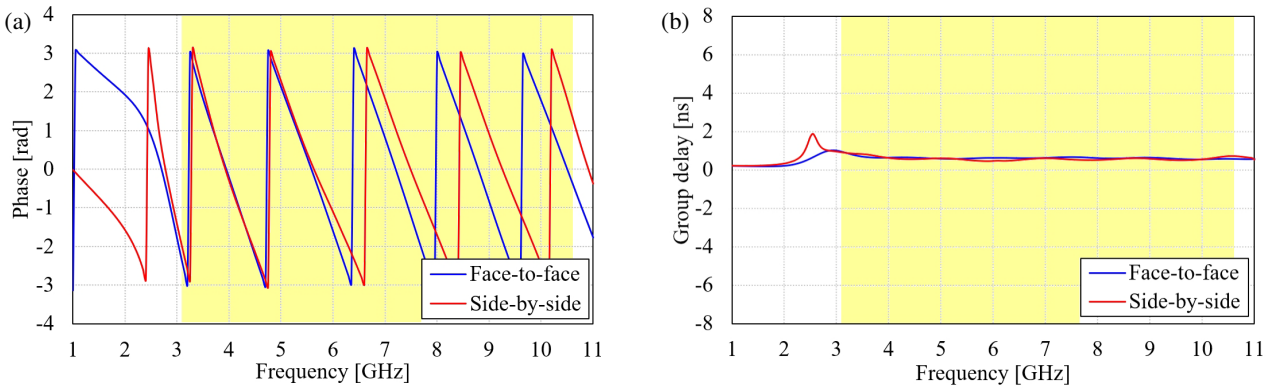

FIGURE 17. Calculated phase and group-delay characteristics of S_{21}: (a) phase and (b) group-delay.

TABLE 1. Quantitative comparison of the proposed antenna with representative compact UWB monopole antennas.

Ref.	Design technique	Antenna size [mm^3]	Antenna substrate	BW [GHz]	Peak gain [dBi]/ Efficiency [%]	Radiation stability	Time-domain analysis
[15]	Square-ring slot-shaped	$120 \times 100 \times 0.5$	RO4003B	3–11	4/NR	Stable radiation	No
[17]	Trapezoidal slot-shaped with via holes	$27 \times 29 \times 1.0$	$\varepsilon_r = 2.65$	3.0–10.6	5.2/NR	Stable radiation	No
[18]	Cactus-shaped	$28 \times 20 \times 0.35$	LCP	2.9–12	5.5/NR	Quasi-omnidirectional	No
[19]	Asymmetric slots on radiator	$21.6 \times 20.8 \times 1.6$	FR-4	2.2–16.5	9.57/higher than 80	Quasi-omnidirectional	Yes
[20]	Modified-hexagonal-shaped	$25 \times 12.5 \times 1$	FR-4	3.1–10.8	4.12/NR	Quasi-omnidirectional	Yes
[21]	Triple band-notched monopole	$40 \times 29 \times 1.6$	FR-4	2.7–11.0	2.88/higher than 80	Quasi-omnidirectional	No
[22]	Circularly-polarized UWB (CMA)	$30 \times 24 \times 1.6$	FR-4	5.7–10.7	5.4/higher than 80	Stable radiation/ CP operation	Yes
[23]	DGS-based wideband monopole	$34 \times 28 \times 1.5$	$\varepsilon_r = 2.2$	4.0–18.9	7.4/NR	Broad main lobe	No
[24]	Ring-structured UWB (CMA)	$35 \times 30 \times 1.6$	FR-4	3.0–11.7	NR/higher than 65	Stable radiation	No
[25]	Slot and modified ground plane	$47 \times 37 \times 1.6$	FR-4	3.1–10.6	3.83/NR	Quasi-omnidirectional	No
[26]	Modified circular planar monopole	$30 \times 20 \times 1.6$	FR-4	2.66–11.0	3.157/maximum 96.6	Quasi-omnidirectional	Yes
[28]	Bell-shaped, short stub	$28 \times 20 \times 1.6$	FR-4	3.1–10.6	4.7/NR	Quasi-omnidirectional	No
[29]	Half bell-shaped, short stub	$30 \times 12 \times 1.6$	FR-4	3.1-10.6	2.4/NR	Quasi-omnidirectional	No
This work	Bell-shaped, coupling, short stub	$24 \times 14 \times 1.6$	FR-4	3.1-10.6	2.5/higher than 84	Quasi-omnidirectional	Yes

NR: Not reported.

balanced performance in terms of its compact size, simple FR-4 implementation, full coverage of the FCC-defined UWB, quasi-omnidirectional radiation, and time-domain stability.

In contrast, the proposed UWB printed monopole antenna has a significantly smaller footprint ($24 \times 14 \times 1.6$ mm) and achieves comparable or superior performance. It relies solely on a standard, low-cost, and widely available FR-4 substrate. The adoption of coupling and short-stub structures enables effective impedance tuning, particularly at the lower end of the UWB. It is typically most difficult to achieve impedance matching with compact designs. This unique approach allows the antenna to maintain a VSWR of ≤ 2 across the entire UWB

(3.1–10.6 GHz) without introducing excessive structural complexity. Furthermore, unlike several compact UWB antennas that suffer from distorted radiation patterns at higher frequencies, the proposed antenna maintains an almost omnidirectional radiation across the UWB. This ensures a reliable performance for mobile and handheld applications. When time-domain metrics such as the correlation coefficient and group delay are also considered, it becomes clear that the proposed antenna demonstrates clear advantages in terms of waveform fidelity and temporal stability.

It should also be noted that the proposed antenna involves several trade-offs. First, using an FR-4 substrate is advantageous in terms of cost and fabrication simplicity, but it can increase dielectric loss compared to low-loss microwave substrates. Second, while the compact, asymmetric coupling-and-stub structure contributes to miniaturization and impedance matching, it may also cause slight distortion of the radiation pattern and increased cross-polarization at higher frequencies. Third, the proposed antenna is designed to cover the FCC-defined UWB rather than to maximize the absolute impedance bandwidth beyond 10.6 GHz. Despite these trade-offs, the proposed antenna is a practical compromise for compact UWB systems because it simultaneously achieves small size, low-cost fabrication, UWB impedance matching, quasi-omnidirectional radiation, and stable time-domain characteristics.

5. CONCLUSIONS

In this paper, a compact printed ultra-wideband (UWB) monopole antenna employing a coupling structure and a short stub has been proposed and experimentally validated. The proposed antenna achieves broadband impedance matching across the entire FCC-defined UWB (3.1–10.6 GHz) while significantly reducing the antenna footprint. By introducing capacitive coupling between the front- and back-side radiating elements and incorporating a short stub for reactive compensation, effective broadband operation is realized without increasing the structural or fabrication complexity.

A parametric investigation clarified the respective roles of the coupling structure and short stub in impedance control. The coupling structure provides capacitive loading to mitigate the impedance degradation caused by miniaturization, whereas the short stub improves impedance matching, particularly at lower frequencies. Consequently, the proposed antenna achieves approximately 40% size reduction compared with previously reported stub-loaded printed monopole antennas while maintaining comparable bandwidth characteristics.

Frequency-domain evaluations confirm that the proposed antenna exhibits a VSWR ≤ 2 and quasi-omnidirectional radiation characteristics over the entire UWB. In addition, time-domain analysis using face-to-face and side-by-side antenna configurations demonstrates high waveform fidelity, with correlation coefficients exceeding 0.94 and a nearly constant group delay of approximately 0.3 ns across the operating band. These results indicate minimal signal distortion and stable temporal behavior, both of which are essential for impulse-based UWB communication systems.

ACKNOWLEDGEMENT

This work was partially supported by JSPS KAKENHI Grant Number JP24K07493.

REFERENCES

[1] Xu, H. and L. Yang, "Ultra-wideband technology: Yesterday, today, and tomorrow," in *2008 IEEE Radio and Wireless Symposium*, 715–718, Orlando, FL, USA, 2008.

[2] Win, M. Z., D. Dardari, A. F. Molisch, W. Wiesbeck, and J. Zhang, "History and applications of UWB," *Proceedings of the IEEE*, Vol. 97, No. 2, 198–204, Feb. 2009.

[3] Pyndiah, R., "An overview of UWB technology," in *2006 IET Seminar on Practical Applications for Wireless Networks*, 65–80, Paris, France, 2006.

[4] Kiminami, K., Hirata, and Shiozawa, "Double-sided printed bow-tie antenna for UWB communications," *IEEE Antennas and Wireless Propagation Letters*, Vol. 3, 152–153, 2004.

[5] Liang, J., C. C. Chiau, X. Chen, and C. G. Parini, "Study of a printed circular disc monopole antenna for UWB systems," *IEEE Transactions on Antennas and Propagation*, Vol. 53, No. 11, 3500–3504, Nov. 2005.

[6] Agrawall, N. P., G. Kumar, and K. P. Ray, "Wide-band planar monopole antennas," *IEEE Transactions on Antennas and Propagation*, Vol. 46, No. 2, 294–295, Feb. 1998.

[7] Evans, J. A. and M. J. Amunann, "Planar trapezoidal and pentagonal monopoles with impedance bandwidths in excess of 10:1," in *IEEE Antennas and Propagation Society International Symposium. 1999 Digest. Held in conjunction with: USNC/URSI National Radio Science Meeting (Cat. No.99CH37010)*, Vol. 3, 1558–1561, Orlando, FL, USA, Jul. 1999.

[8] Taniguchi, T. and T. Kobayashi, "An omnidirectional and low-VSWR antenna for the FCC-approved UWB frequency band," in *IEEE Antennas and Propagation Society International Symposium. Digest. Held in conjunction with: USNC/CNC/URSI North American Radio Sci. Meeting (Cat. No.03CH37450)*, Vol. 3, 460–463, Columbus, OH, USA, Jun. 2003.

[9] Su, S.-W., K.-L. Wong, and C.-L. Tang, "Ultra-wideband square planar monopole antenna for IEEE 802.16a operation in the 2–11-GHz band," *Microwave and Optical Technology Letters*, Vol. 42, No. 6, 463–466, Jul. 2004.

[10] Antonino-Daviu, E., M. Cabedo-Fabrés, M. Ferrando-Bataller, and A. Valero-Nogueira, "Wideband double-fed planar monopole antennas," *Electronics Letters*, Vol. 39, No. 23, 1635–1636, Nov. 2003.

[11] Wong, K.-L., C.-H. Wu, and S.-W. Su, "Ultrawide-band square planar metal-plate monopole antenna with a trident-shaped feeding strip," *IEEE Transactions on Antennas and Propagation*, Vol. 53, No. 4, 1262–1269, Apr. 2005.

[12] Srifi, M. N., S. K. Podilchak, M. Essaaidi, and Y. M. M. Antar, "Planar circular disc monopole antennas using compact impedance matching networks for ultra-wideband (UWB) applications," in *2009 Asia Pacific Microwave Conference*, 782–785, Singapore, Dec. 2009.

[13] Koshiji, F., S. Itaya, Y. Akiyama, and K. Koshiji, "Proposal and investigation of miniaturizing unbalanced dipole antenna for ultra wideband radio," *Journal of the Japan Institute of Electronics Packaging*, Vol. 15, No. 7, 526–533, 2012.

[14] Abbosh, A. M., "Miniaturization of planar ultrawideband antenna via corrugation," *IEEE Antennas and Wireless Propagation Letters*, Vol. 7, 685–688, 2008.

[15] Sadat, S., M. Fardis, F. Geran, G. Dadashzadeh, N. Hojjat, and M. Roshandel, "A compact microstrip square-ring slot antenna for UWB applications," in *2006 IEEE Antennas and Propagation Society International Symposium*, 4629–4632, Albuquerque, NM, USA, Jul. 2006.

[16] Azim, R., M. T. Islam, and N. Misran, "Compact tapered-shape slot antenna for UWB applications," *IEEE Antennas and Wireless Propagation Letters*, Vol. 10, 1190–1193, Oct. 2011.

[17] Chen, D. and C.-H. Cheng, "A novel compact ultra-wideband (UWB) wide slot antenna with via holes," *Progress In Electromagnetics Research*, Vol. 94, 343–349, 2009.

[18] Nikolaou, S. and M. A. B. Abbasi, "Miniaturization of UWB antennas on organic material," *International Journal of Antennas and Propagation*, Vol. 2016, No. 1, 5949254, 2016.

[19] Kempanna, S. B., R. C. Biradar, T. Ali, V. K. Jhunjhunwala, S. Soman, and S. Pathan, "A compact slotted UWB antenna based on characteristics mode theory for wireless applications," *Designs*, Vol. 7, No. 6, 141, Dec. 2023.

[20] Park, S. and K.-Y. Jung, "Novel compact UWB planar monopole antenna using a ribbon-shaped slot," *IEEE Access*, Vol. 10, 61 951–61 959, Jun. 2022.

[21] Lin, H., Z. Lu, Z. Wang, and W. Mu, "A compact UWB monopole antenna with triple band notches," *Micromachines*, Vol. 14, No. 3, 518, 2023.

[22] Heo, H., M.-J. Kang, S. Park, J. Lee, L. Qu, and K.-Y. Jung, "Design of a UWB circularly-polarized planar monopole antenna using characteristic mode analysis," *Scientific Reports*, Vol. 14, No. 1, 26236, 2024.

[23] Tsegaye, A., X.-Q. Lin, H. Liu, and H. S. Abubakar, "A compact monopole wideband antenna based on DGS," *Electronics*, Vol. 14, No. 12, 2311, 2025.

[24] Xiang, Z., Z. Wang, C. Li, and R. You, "Design of UWB monopole antenna with ring structure based on characteristic mode theory," *Progress In Electromagnetics Research C*, Vol. 158, 225–234, 2025.

[25] Jansri, C., C. Phongcharoenpanich, and S. Lamultree, "A printed circular monopole antenna with slot and modified ground plane for UWB applications," in *2018 15th International Conference on Electrical Engineering/Electronics, Computer, Telecommunications and Information Technology (ECTI-CON)*, 564–567, Chiang Rai, Thailand, 2018.

[26] Anveshkumar, N. and A. S. Gandhi, "Design and performance analysis of a modified circular planar monopole UWB antenna," in *2017 8th International Conference on Computing, Communication and Networking Technologies (ICCCNT)*, 1–5, Delhi, India, 2017.

[27] Guo, Q., J. Zhang, Y. Wang, and C. Song, "Investigation of graphene film-based circular monopole antenna for UWB applications," in *2019 Computing, Communications and IoT Applications (ComComAp)*, 361–364, Shenzhen, China, 2019.

[28] Takemura, N. and S. Ichikawa, "Broadbanding of printed bell-shaped monopole antenna by using short stub for UWB applications," *Progress In Electromagnetics Research C*, Vol. 78, 57–67, 2017.

[29] Takemura, N., "Design and experimental evaluation of a compact half-shaped printed-monopole antenna with short stub for UWB systems," *Progress In Electromagnetics Research C*, Vol. 165, 1–10, 2026.

[30] Takemura, N., "Design and experimental evaluation of a miniaturized printed UWB monopole antenna employing a coupling and stub structure," in *2026 IEEE International Workshop on Antenna Technology (iWAT)*, 1–2, Liverpool, United Kingdom, Mar. 2026.

[31] Pele, I., A. Chousseaud, and S. Toutain, "Simultaneous modeling of impedance and radiation pattern antenna for UWB pulse modulation," in *2004 IEEE Antennas and Propagation Society Symposium*, Vol. 2, 1871–1874, Monterey, CA, USA, Jun. 2004.